JACS
JOURNAL OF THE AMERICAN CHEMICAL SOCIETY
Article
pubs.acs.org/JACS

Block Co-PolyMOCs by Stepwise Self-Assembly

Yufeng Wang,[†] Mingjiang Zhong,[†] Jiwon V. Park,[†] Aleksandr V. Zhukhovitskiy,[†] Weichao Shi,[‡] and Jeremiah A. Johnson*[,†]

[†]Department of Chemistry, Massachusetts Institute of Technology, 77 Massachusetts Avenue, Cambridge, Massachusetts 02139, United States

[‡]John A. Paulson School of Engineering and Applied Sciences, Harvard University, Cambridge, Massachusetts 02138, United States

Supporting Information

ABSTRACT: We report a stepwise assembly strategy for the integration of metal−organic cages (MOCs) into block copolymers (BCPs). This approach creates "block co-polyMOC" (BCPMOC) materials whose microscopic structures and mechanical properties are readily tunable by adjusting the size and geometry of the MOCs and the composition of the BCPs. In the first assembly step, BCPs functionalized with a pyridyl ligand on the chain end form star-shaped polymers triggered by metal-coordination-induced MOC assembly. The type of MOC junction employed precisely determines the number of arms for the star polymer. In the second step, microphase separation of the BCP is induced, physically cross-linking the star polymers and producing the desired BCPMOC networks in the bulk or gel state. We demonstrate that large spherical $M_{12}L_{24}$ MOCs, small paddlewheel M_2L_4 MOCs, or a mixture of both can be incorporated into BCPMOCs to provide materials with tailored branch functionality, phase separation, microdomain spacing, and mechanical properties. Given the synthetic and functional diversity of MOCs and BCPs, our method should enable access to BCPMOCs for a wide range of applications.

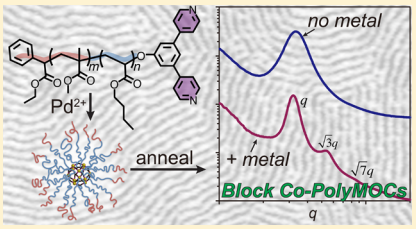

INTRODUCTION

Coordination-directed self-assembly of metal ions and organic ligands is a powerful approach for the construction of two- and three-dimensional molecular architectures.[1−10] Examples of such structures range from discrete metal−organic cycles and metal−organic cages/polyhedra (MOCs/MOPs)[11−27] to infinite metal−organic frameworks (MOFs).[28−31] By rational design of the ligands and proper choice of the metal ions, these materials can feature well-defined sizes, shapes, geometries, and porosity, which enable applications in selective encapsulation, catalysis, sensing, etc.[32−40]

Inspired by the structural versatility as well as the dynamic nature of metal coordination, much effort has recently been devoted to the introduction of metal−organic structures, which are generally rigid, into elastic polymer networks. The goal is to synthesize a new class of hybrid materials that have tunable viscoelastic properties and are capable of realizing multiple functions originally only possible for MOFs and MOCs.[41−46] For example, in 2015 we reported on the synthesis of polyethylene glycol (PEG) hydrogels cross-linked via metal-losupramolecular assembly of M_xL_y clusters (x metal ions and y ligands for each junction; M_4L_4 squares were targeted)[47] derived from bispyridyl tetrazine ligands bound to the ends of PEG chains and either Fe^{2+} or Ni^{2+} ions.[48] These gels were used as scaffolds for controlled photoinduced drug release and enzymatic reactions. In the same year, Nitschke and co-workers synthesized PEG hydrogels by cross-linking PEG chains with M_4L_6 pyramidal MOC junctions.[49] Small molecules, benzene and furan, could be encapsulated and released from the MOCs in these materials. In 2016, Yang and co-workers reported a postassembly polymerization strategy to combine thermoresponsive polymers with small metallacyles to yield hydrogels with self-healing properties.[50] Later, Kitagawa and co-workers reported the synthesis of coordination star polymers containing copper-based MOCs using both divergent and convergent methods.[51]

Recently, we described the assembly of polymeric organogels connected with MOC junctions.[52] These "polyMOC" gels featured large MOCs, for instance, the $M_{12}L_{24}$ spherical "Fujita cages", which served as cross-link junctions between linear polymer chains. Because the polymers used had ligands on both of their ends, the resulting network was assembled in one step, which produced polyMOCs with a high percentage of topological defects. However, the use of large MOC junctions enabled the network to withstand those defects and at the same time allowed for the introduction of additional functionality via exchange of elastically inactive loops with functional free ligands.

Building on these efforts, we envisioned the merger of MOCs with a classic paradigm in polymer science: block copolymer (BCP) self-assembly.[53−55] BCP assembly is a widely employed "bottom-up" method for the fabrication of materials with periodic structures on the order of ∼10−100 nm. Since MOCs are generally an order of magnitude smaller than this size range, we reasoned that hybrid materials based on MOC and BCP assembly could feature unique hierarchical structures with properties defined by order across various length scales. Such

Received: June 29, 2016
Published: July 27, 2016

DOI: 10.1021/jacs.6b06712
J. Am. Chem. Soc. 2016, 138, 10708−10715

structural hierarchy is common in biomaterials, but is often more difficult to achieve in synthetic polymers.

Herein, we introduce block co-polyMOCs (BCPMOCs), which are a class of materials derived from stepwise MOC assembly and BCP phase separation. Our BCPMOCs are constructed from BCPs that feature one glassy block, one rubbery block, and a pyridyl ligand on the end of the rubbery block (Figure 1a). These BCPs undergo metal-coordination-driven assembly in solution to yield star polymers with well-defined MOC cores and a precise number of polymer arms. When the solvent is removed, or a solvent that is selective for one block of the BCP is added, these materials undergo phase separation and physical cross-linking by forming glassy polymer domains to yield BCPMOCs as thermoplastic elastomers (TPE) or thermoresponsive organogels. We demonstrate the synthesis of BCPMOCs with large (~3.5 nm) Fujita-sphere $M_{12}L_{24}$ MOCs and small (~1.5 nm) paddlewheel M_2L_4 MOCs. Since the conformations of attached BCP chains are restricted differently depending on the MOC, BCPMOCs derived from these two MOCs have different microphase-separated structures; i.e., MOC assembly at short length scales impacts BCP assembly at longer length scales. Furthermore, we show that the structures and mechanical properties of BCPMOCs are highly tunable and directly related to the MOC and the BCP.

To the best of our knowledge, this work represents the first example wherein MOC assembly is merged with BCP phase separation to generate cross-linked materials. The versatility of MOC assembly and the rich diversity of potential BCP structures and compositions provide great opportunities to develop novel BCPMOCs with a range of properties. For example, herein we show that BCPs with a thermosensitive block can be employed to fabricate thermoresponsive BCPMOC organogels.

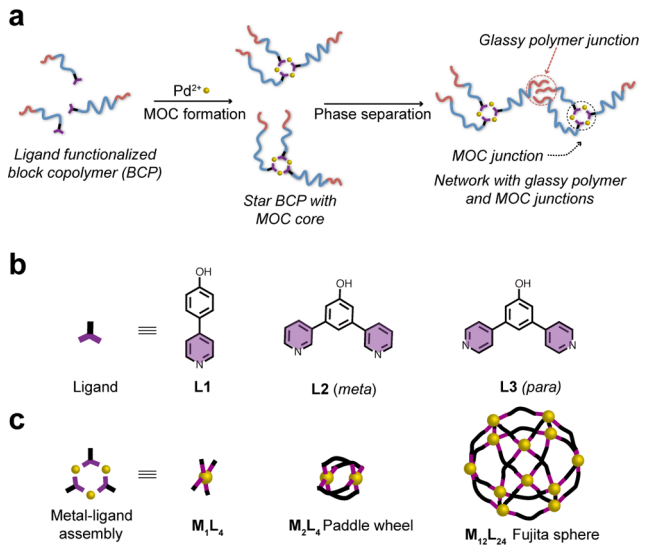

Figure 1. (a) Scheme showing the stepwise self-assembly of BCPMOCs by MOC formation followed by BCP phase separation. (b) Schematic and chemical structures of ligands employed to form MOCs. (c) Schematic representation of the sizes and geometries in metal–ligand assemblies investigated.

RESULTS AND DISCUSSION

For the realization of BCPMOCs, we used poly(methyl methacrylate)-*block*-poly(*n*-butyl acrylate) (**PMMA-*b*-PBA**, or **PMMA-PBA**) bearing a pyridyl ligand at the chain end. **PMMA-PBA** is known to phase separate in the bulk state as well as in suitable solvents.[56,57] Our ligands of choice are shown in Figure 1b. In the presence of Pd^{2+} ions, these ligands form

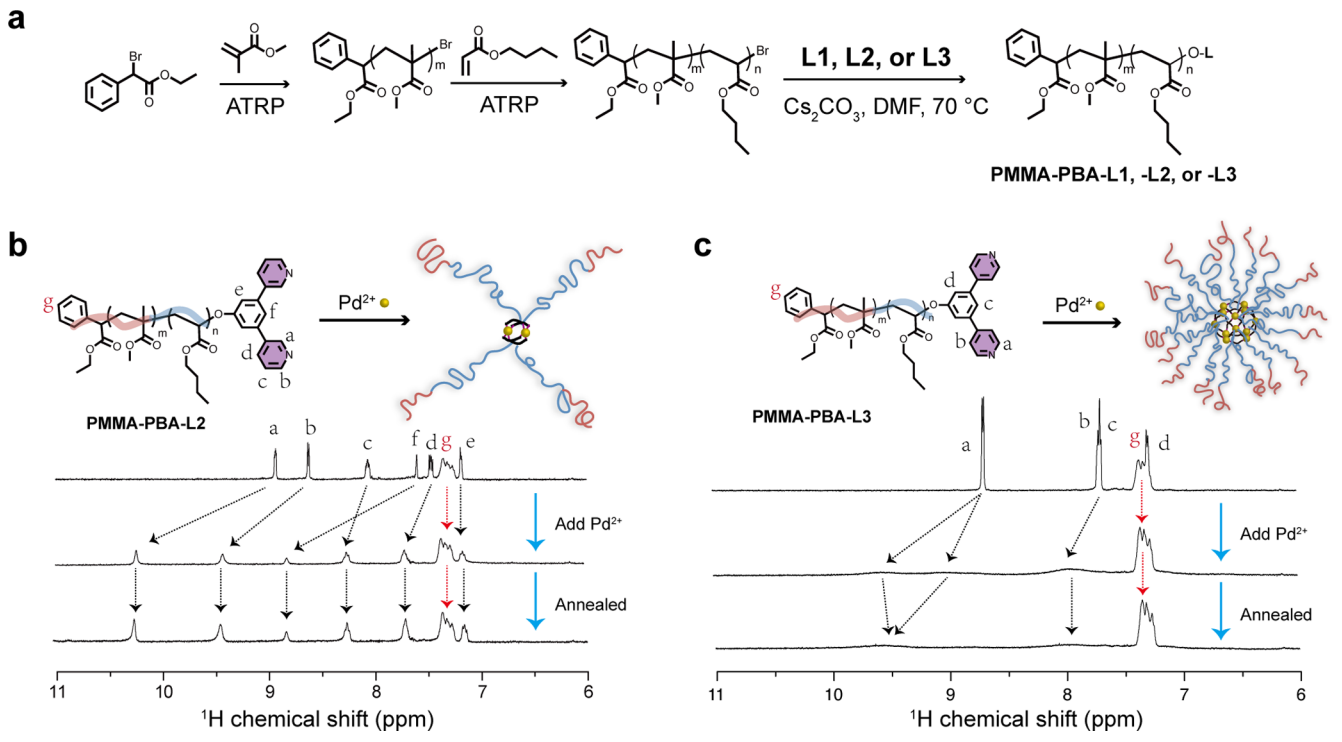

Figure 2. Synthetic scheme of pyridyl ligand functionalized poly(methyl methacrylate)-*block*-poly(*n*-butyl acrylate) (**PMMA-PBA-L**). (b) ^{1}H NMR characterization of the self-assembly of **PMMA-PBA-L2** to form 4-arm star polymers containing a paddlewheel MOC core. (c) ^{1}H NMR characterization of the self-assembly of **PMMA-PBA-L3** into 24-arm star polymers with a Fujita-sphere MOC core.

DOI: 10.1021/jacs.6b06712
J. Am. Chem. Soc. 2016, 138, 10708–10715

Pd_xL_y complexes with different geometries: ligand **L1** forms a square-planar ML_4 complex (this ligand serves as a control for comparison to BCPMOCs), while ligands **L2** and **L3** are structural isomers of *meta*- and *para*-bispyridine that assemble into M_2L_4 paddlewheel and $M_{12}L_{24}$ Fujita-sphere MOCs, respectively. Schematics for these complexes are shown in Figure 1c.

BCP Synthesis. The BCPs were synthesized via atom transfer radical polymerization (ATRP), followed by post-polymerization functionalization (Figure 2a). Using ethyl α-bromophenylacetate (EBPA) as the initiator, the PMMA block could be synthesized with low dispersities ($Đ$ = 1.05−1.10) and controlled molecular weights.[58] The obtained PMMA then served as a macroinitiator for the synthesis of **PMMA-PBA** through chain extension. To install the desired ligand on the PBA chain end, we used a nucleophilic substitution reaction in which the appropriate pyridyl phenol ligand displaced the polymer chain-end bromide to yield an ether product. The functionalized polymers were purified by silica gel chromatography (Supporting Information, SI). ^{1}H nuclear magnetic resonance spectroscopy (^{1}H NMR) confirmed the presence of protons from both the EBPA initiator and the bispyridine chain end, as labeled in Figure 2b,c. The integration of characteristic peaks for all three macroligands agrees well with the chemical structures, which suggests a high degree (>95%) of chain-end functionalization (Figure S1). Apart from the difference in the ligands, we synthesized BCPs of different molecular weights and block volume fractions for comparison; detailed characterization data for all polymers studied are listed in Table 1. For nomenclature, **$PMMA_{4k}$-PBA_{19k}-L1** stands for BCPs with a number-average molecular weight of 4k and 19k for each block and ligand **L1** as the chain end (also abbreviated as **−L1** in the same context).

Table 1. Characterization Data for BCPs

polymer[a]	M_n[b]	$Đ$[c]	N_{PMMA}[d]	f_{PMMA}[e]	N_{PBA}[d]	f_{PBA}[e]
$PMMA_{4k}$-PBA_{19k}	22.9k	1.14	39	16.4	147	83.6
$PMMA_{8k}$-PBA_{27k}	34.1k	1.07	82	23.1	221	76.9
$PMMA_{8k}$-PBA_{48k}	52.1k	1.09	82	14.8	385	85.2

[a]Sample names and number-average molecular weights (M_n) determined by ^{1}H NMR. [b]M_n measured by GPC. [c]Dispersity index (M_w/M_n) measured by GPC. [d]Degree of polymerization (N) determined by ^{1}H NMR. [e]Volume fraction (f) calculated on the basis of N and the density of PMMA and PBA.

Metal-Coordination-Driven MOC Assembly. When palladium nitrate is introduced to a solution of **PMMA-PBA-L** in acetonitrile, Pd−pyridine coordination occurs rapidly to give poorly defined coordination polymer networks. However, upon thermal annealing, the BCP-bound ligands and Pd^{2+} ions assemble into the clusters shown schematically in Figure 1c. We used ^{1}H NMR to study the assembly process as well as the differences between polymers bearing various chain ends. **$PMMA_{4k}$-PBA_{19k}** polymers are used as examples. The ^{1}H NMR spectra for *meta*-bispyridyl **L2** functionalized polymer (**$PMMA_{4k}$-PBA_{19k}-L2**) are shown in Figure 2b. When Pd^{2+} is added, most of the peaks corresponding to the ligand shift downfield. In particular, the peaks for the α pyridyl protons (labeled as a and b in Figure 2b) shift from 8.9 to 10.5 ppm, and 8.6 to 9.4 ppm, respectively. The new chemical shifts agree with those obtained from a model study using small molecules (Figure S2), which supports the assembly of paddlewheel junctions. Annealing of the sample at 80 °C for 4 h renders a sharper set of peaks, indicative of the formation of 4-arm polymers with well-defined cage structures. Because they are far from the MOC junction, the peaks for the EBPA initiator (labeled as g in Figure 2b) do not change before and after the assembly.

The *para*-bispyridyl **L3** functionalized polymer (**$PMMA_{4k}$-PBA_{19k}-L3**) showed a completely different NMR spectrum in the aromatic region when assembled with Pd^{2+} (Figure 2c). The originally sharp peaks for the ligand turned into multiple broad peaks and shifted downfield. For example, the peak at 8.7 ppm for the α pyridyl proton (labeled as a in Figure 2c) is split to two peaks at 9.1 and 9.5 ppm. Prior to annealing, it is known that **L3** as a small molecule can form kinetically trapped clusters with many different sizes and configurations when assembled with Pd^{2+}.[52,59] These ill-defined structures significantly broaden the corresponding NMR peaks. After annealing, the peak at 9.1 ppm merges together with the peak at 9.5 ppm, which suggests that the system has reorganized. The fact that the final chemical shifts agree with ones obtained from the analogous non-polymeric ligand (Figure S3) supports the formation of the $M_{12}L_{24}$ MOC. Because the MOC is buried in 24 polymer chains, it is difficult to resolve by ^{1}H NMR (broad peaks) due to slowed relaxation and peak broadening. In contrast, the EBPA initiator residues located on the periphery of the star polymer are clearly observed (labeled as g in Figure 2c).

Dynamic light scattering (DLS) was used to confirm the formation of star polymers with each MOC core. As shown in Figure 3a, particles with a diameter of 12 ± 2 nm were observed for star polymers with a paddlewheel core (top image). For polymers with the $M_{12}L_{24}$ MOC junction, the diameter was 23 ± 4 nm (bottom image). In both cases, the particles have a narrow size distribution. We estimated the radius of gyration (R_g) of these star polymers based on the molecular weight of the constitutive linear polymers and the number of arms using an ideal chain model (see SI for calculation).[60] The values of $2R_g$ for the 4-arm and 24-arm star polymers were 12.5 and 21.3 nm, respectively, which agree with the trend of hydrodynamic diameter (D_h) measured by DLS. Thus, though the BCP component is the same in both systems, and the MOCs themselves only differ in size by ∼2 nm, the MOC structure significantly impacts the star polymer size.

We employed atomic force microscopy (AFM) to visualize the star polymers with the large $M_{12}L_{24}$ cores. Figure 3b shows a typical 3D height image of **$PMMA_{4k}$-PBA_{19k}-L3** after annealing with Pd^{2+} and spin-coating onto the surface of a silicon wafer. Relatively uniform particles of about 40 ± 8 nm in diameter were observed (Figure 3b). The heights of the particles ranged from 1.5 to 2.8 nm, slightly smaller than what has been measured for the Fujita spheres (∼3.5 nm),[61] which we attribute to the fact that when the star polymer dries on the substrate, the cages collapse due to stretching of the tethered BCP chains. Polymer stretching and spreading on the surface also account for the discrepancy between the particle sizes measured using DLS and AFM. To rule out the possibility that the observed nanoparticles are the result of micelle formation of the BCP itself, a control experiment was conducted with BCPs at the same concentration but in the absence of Pd^{2+}. In this case, no particles were found (Figure S4). These observations were further verified by transmission electron microscopy (TEM), which revealed ∼35 ± 6 nm nanoparticles for $M_{12}L_{24}$ star polymers derived from **$PMMA_{4k}$-PBA-$_{19k}$-L3**. Due to their

DOI: 10.1021/jacs.6b06712
J. Am. Chem. Soc. 2016, 138, 10708−10715

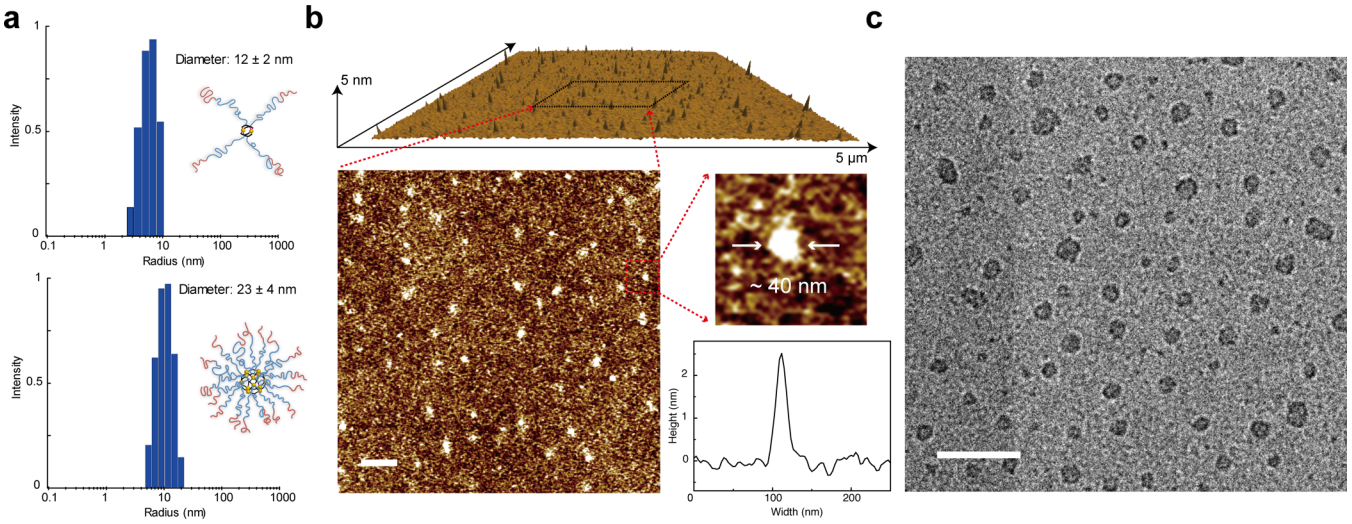

Figure 3. (a) Dynamic light scattering (DLS) histograms showing the size and size distribution of 4-arm (top) and 24-arm (bottom) star polymers assembled using **PMMA-PBA-L2** and **-L3**. (b) Atomic force microscopy (AFM) height images showing the star polymers nanoparticle containing a Fujita-sphere MOC core. (b) Selected area is zoomed in, and the height profile for a selected particle is depicted showing its width and height. (c) Transmission electron microscope image showing the same particles used in part b. Scale bars, 200 nm.

small size, the four-arm star polymers bearing a paddlewheel MOC core were not observable using either AFM or TEM.

BCPMOC Formation by BCP Phase Separation. Having shown that MOC assembly can be used to drive the formation of star polymers in solution with precise sizes and numbers of BCP arms, we sought to leverage BCP phase separation and attractive interactions between the PMMA blocks to cross-link these star polymers and provide BCPMOCs (Figure 1a). In this event, solvent was evaporated, and the resulting bulk materials were thermally annealed to induce microphase separation of the BCPs and generate glassy PMMA microdomains. Together with the MOC junctions, the PMMA microdomains serve as physical cross-links to give elastic BCPMOC networks, or BCPMOC TPEs (Figure 1a).

Small-angle X-ray scattering analysis (SAXS) was used to study the microphase separation. The SAXS diffractograms of the linear BCP **PMMA$_{4k}$-PBA$_{19k}$** (~16% PMMA) without metal and **PMMA$_{4k}$-PBA$_{19k}$-L1** with metal are shown in Figure 4a (left, blue and red trace). For both samples, a single Bragg reflection peak located at q = 0.046 Å^{-1} is observed, indicating phase-separated structures with a d-spacing, i.e., the distance between adjacent PMMA-rich domains, equal to 13.7 nm. In this case, the coordination of Pd^{2+} by the monopyridine chain ends has little effect on the BCP assembly.

The scattering profiles for the BCPMOCs consisting of identical polymer backbone but different MOC cores (i.e., **PMMA$_{4k}$-PBA$_{19k}$-L2** and **-L3**) are shown (Figure 4a, left). Two Bragg peaks are observed for each BCPMOC, which suggests that the incorporation of MOCs can facilitate phase separation and long-range ordering of the materials. Similar phenomena have been observed in other types of star polymer systems.[62] The d-spacing calculated on the basis of the position of the principal peak is 15.0 nm for both **-L2** and **-L3**, an increase of 1.3 nm compared to the linear polymer due to polymer chain stretching in a star-like structure when the two blocks phase separate. The q ratio for the second peak to the primary peak is $q2/q1 = 1:\sqrt{3}$, suggesting a sphere or a hexagonally packed cylinder morphology; the exact morphology of this BCPMOC cannot be assigned due to a limited number of higher order peaks.

We used AFM to visualize the phase-separated morphology. The linear **PMMA$_{4k}$-PBA$_{19k}$** does not show appreciable contrast in the phase profile mainly because the molecular weight of the polymer is low (Figure S5), while for **PMMA$_{4k}$-PBA$_{19k}$-L3** bearing the spherical cages, contrast between the two blocks is observed (Figure 4a, middle).

The mechanical properties of these materials were probed by oscillatory rheometry. For **PMMA$_{4k}$-PBA$_{19k}$** alone, the storage modulus G' was similar to the loss modulus G''. At lower angular frequencies, G' was smaller than G'', while at higher frequencies (ω > 20 rad/s), G' was slightly greater than G''; the polymer behaves as a very viscous fluid (Figure 4a, right, blue trace). In contrast, all of the metal-coordinated materials derived from **PMMA$_{4k}$-PBA$_{19k}$-L** were elastic at all frequencies; the G' values increased and were significantly larger than G''. The extent to which G' increased depended on the geometry of the MOC. For **PMMA$_{4k}$-PBA$_{19k}$-L3** bearing the Fujita-sphere MOC, G' (at 0.1 rad/s, same thereafter) reached as high as 170 kPa, while the values for **PMMA$_{4k}$-PBA$_{19k}$-L1** and **-L2** were 29.4 and 89.3 kPa, respectively. According to the phantom network theory,[60] the difference in shear moduli can be attributed to the fact that the branch functionality in these BCPMOCs is increasing, from f = 4 for **-L1** and **-L2** to f = 24 for **-L3**. Furthermore, networks prepared from **-L3** may be more uniform as indicated by SAXS, and thus, they may possess fewer elastically ineffective defects.[63] Although in principle materials bearing ligands **L1** and **L2** have the same branch functionality, we find that the material with **L1** is much softer (smaller G'). This observation suggests that the square-planar junctions in the **L1**-based material are more dynamic than the M_2L_4 junctions in the **L2**-based BCPMOC.[64]

We also studied the role of the BCP composition, i.e., **PMMA$_{8k}$-PBA$_{27k}$** and **PMMA$_{8k}$-PBA$_{48k}$**, on the BCPMOC properties. For BCPMOCs based on **PMMA$_{8k}$-PBA$_{27k}$**, which has a higher molecular weight and a slightly larger fraction of PMMA (~23% PMMA), a similar trend is observed where materials with larger MOC junctions exhibit long-range ordering, as evidenced by the sharpening (for **PMMA$_{8k}$-PBA$_{27k}$-L1**) and the presence of higher order scattering peaks (for **PMMA$_{8k}$-PBA$_{27k}$-L2 and -L3**) in SAXS (Figure 4b). The

DOI: 10.1021/jacs.6b06712
J. Am. Chem. Soc. 2016, 138, 10708−10715

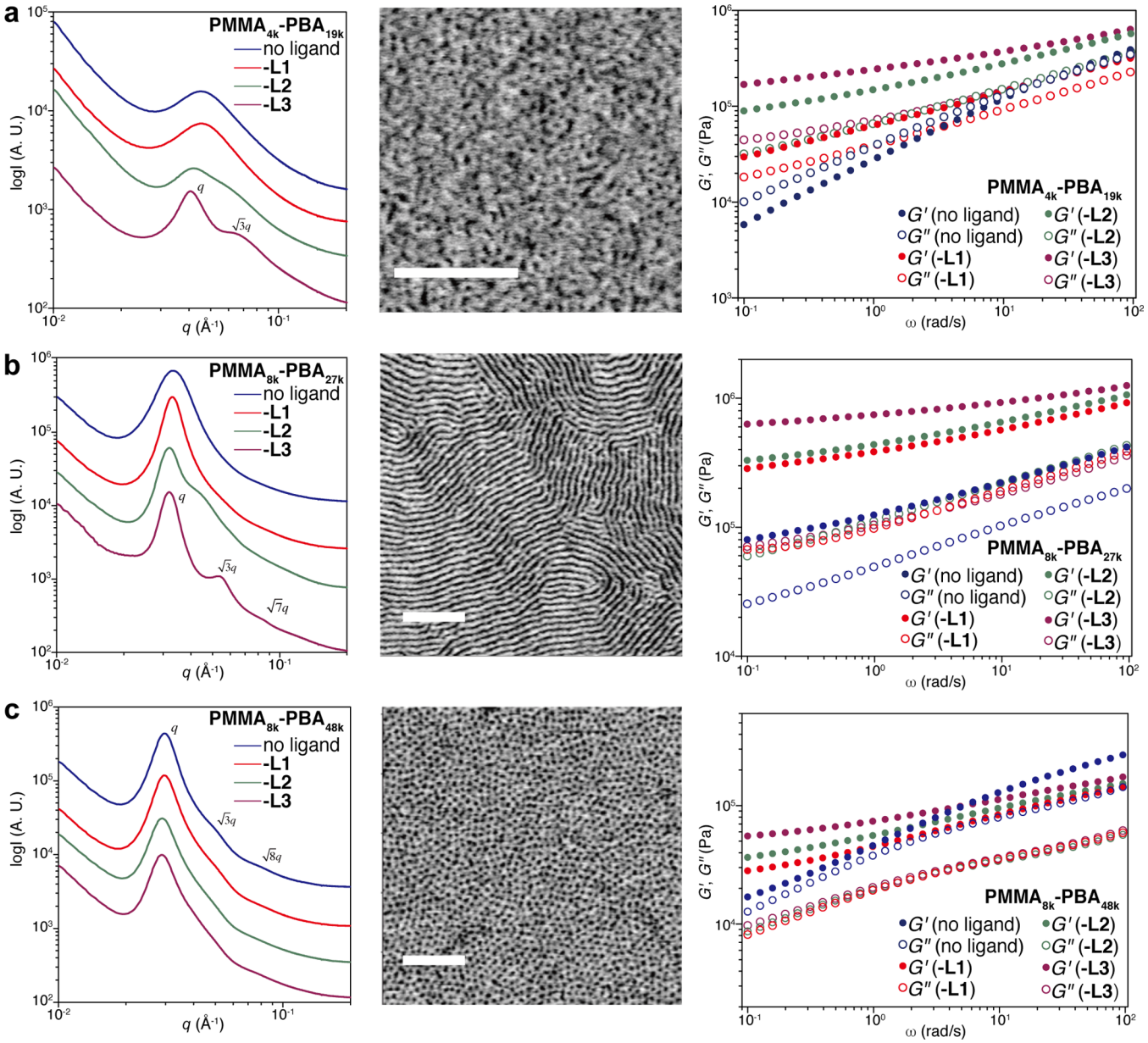

Figure 4. Small-angle X-ray scattering (left), atomic force microscopy (AFM, middle), and rheology study of linear BCPs (blue) and star BCPs with MOCs (red for **-L1**, green for **-L2**, and purple for **-L3**) of different molecular weights and block volume fractions: (a) **PMMA$_{4k}$-PBA$_{19k}$**, (b) **PMMA$_{8k}$-PBA$_{27k}$**, (c) **PMMA$_{8k}$-PBA$_{48k}$**. AFM images for **-L3** samples are shown. Scale bars, 200 nm.

d-spacing for **PMMA$_{8k}$-PBA$_{27k}$-L2** and **-L3** with MOC cores is 19.8 nm, which is 1.0 nm larger than the domain size of the linear **PMMA$_{8k}$-PBA$_{27k}$**, 18.8 nm (Figure 4b, left). For **PMMA$_{8k}$-PBA$_{27k}$-L3** with the Fujita-sphere MOC, the scattering pattern follows $q1{:}q2{:}q3 = 1{:}\sqrt{3}{:}\sqrt{7}$, indicating a hexagonally packed cylinder phase. The AFM phase images of the **PMMA$_{8k}$-PBA$_{27k}$** BCP and polyMOCs are shown in Figure 4b (middle) and Figure S6. They all show the hexagonal cylinder phase, agreeing with the SAXS result. Compared to the BCP, which showed curved cylinders (Figure S6a), the polyMOCs, in particular the **PMMA$_{8k}$-PBA$_{27k}$-L3**, showed longer-range ordering as indicated by the relatively straight cylinders (Figure 4b, middle).

The mechanical properties of BCPMOCs derived from **PMMA$_{8k}$-PBA$_{27k}$** followed similar trends to those based on **PMMA$_{4k}$-PBA$_{19k}$**: the larger the MOC core was, the higher the G' values were (Figure 4b, right). The G' values at 0.1 rad/s for linear **PMMA$_{8k}$-PBA$_{27k}$** and polyMOCs **PMMA$_{8k}$-PBA$_{27k}$-L1**, **-L2**, and **-L3** were 70.7, 284, 329, and 628 kPa, respectively.

In the case of **PMMA$_{8k}$-PBA$_{48k}$** materials, the volume fraction of the PBA block is increased while the molecular weight of PMMA is kept as 8k (~15% PMMA). In contrast to the samples discussed above, the SAXS profiles for these materials show negligible differences between the polymer **PMMA$_{8K}$-PBA$_{48k}$** and materials derived from **PMMA$_{8k}$-PBA$_{48k}$-L1**, **-L2**, or **-L3**. The scattering peaks for all the samples could be indexed as $q1{:}q2{:}q3 = 1{:}\sqrt{3}{:}\sqrt{8}$, implying a spherical morphology (Figure 4c, left). The *d*-spacing based on the principle peak is 21.2 nm. AFM phase images, as shown in Figure 4c (middle) and Figure S7, reveal the same morphology.

For these **PMMA$_{8k}$-PBA$_{48k}$** materials, the degree of polymerization of PBA was increased to ~385 while the size of the PMMA block was kept constant. In this case, the PBA block is large enough to undergo significant chain entanglement (the

DOI: 10.1021/jacs.6b06712
J. Am. Chem. Soc. 2016, 138, 10708−10715

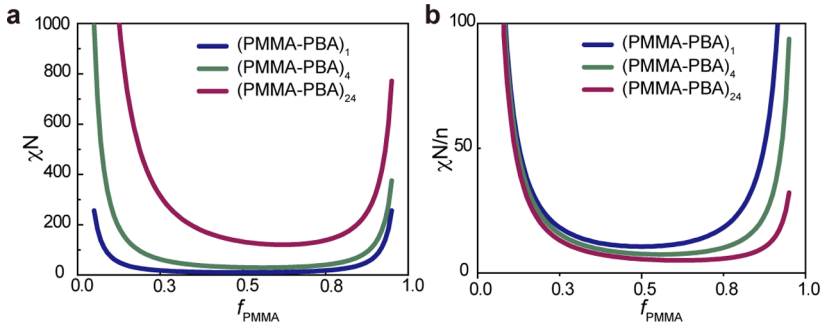

Figure 5. Calculated spinodal curves of star polymers with 1, 4, and 24 **PMMA-PBA** arms. The curve boundary becomes asymmetric with increased number of arms.

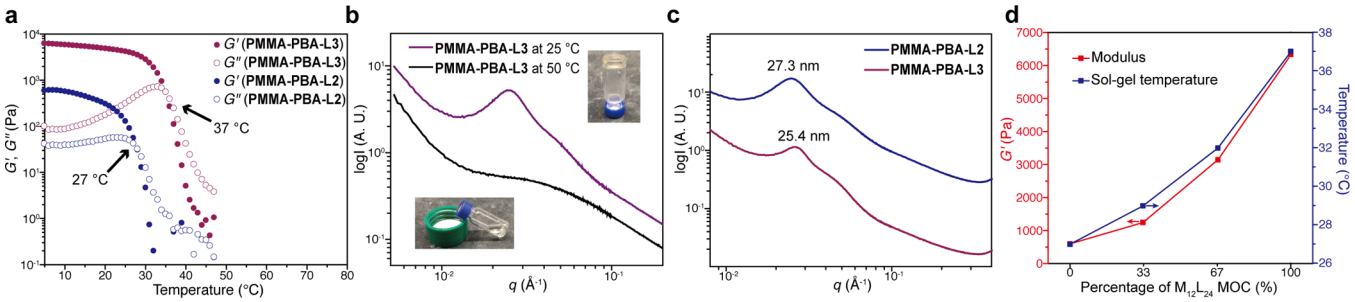

Figure 6. (a) Storage and loss moduli of BCPMOC materials over different temperatures showing the transition between the gel and solution state. (b) SAXS profiles and pictures (inset) for BCPMOCs in 2-ethyl hexanol at 25 °C and 50 °C. (c) SAXS profiles showing the difference in the *d*-spacing of phase separation in gels with different MOC cores. (d) The storage moduli and the sol−gel transition temperature of gels with MOC cores mixed at different ratios.

entanglement molecular weight of PBA in melt is 29k; DP, 226),[65] which leads to an increase of G' for the linear polymer at higher frequency. In the case of the BCPMOCs derived from this polymer, the PBA chain ends are anchored together to MOC cores. This clustering limits chain entanglement, as revealed by the rheology profile in which the G' values do not increase as rapidly with frequency. Again, the type of MOC involved influences the mechanical properties of the BCPMOC. The G' value for the BCPMOC based on the $M_{12}L_{24}$ MOC was greater than that for paddlewheels and monopyridine materials (Figure 4c, right).

Collectively, our data indicate that the structure of the MOC in each BCPMOC dramatically affects the mechanical properties, and in two of three cases the BCP phase separation, compared to either free BCP or the square-planar complex forming system based on **L1**. To rationalize the role of the MOC in BCPMOC phase separation, we used mean field theory with random phase approximation to calculate the spinodal boundaries of the BCPs taking into consideration the difference in the assembly architectures including linear and MOC containing polymers (SI).[66,67] According to the branch functionality, we generalize all polymers as $(\mathbf{PMMA\text{-}PBA})_n$, where n represents the number of BCPs attached to each MOC. For instance, in the case of the star polymers with the spherical and the paddlewheel MOC cores, n = 24 and 4, respectively, while in the case of the linear polymer, n = 1. The calculated spinodal curve is shown in Figure 5, where χ is the Flory−Huggins interaction parameter, N is the total degree of polymerization of the star polymer, and f_{PMMA} is the volume fraction of the PMMA block.

As shown in Figure 5a, when n increases from 1 to 4 and then to 24, the curve boundary shifts upward, and it becomes asymmetric with the boundary more tilted to the higher f_{PMMA} side. This shift means that microphase separation is more likely to occur at higher f_{PMMA} values for the BCPMOCs with larger MOCs. The tendency is more clearly presented when the spinodal curves are normalized by n (Figure 5b).

The asymmetric spinodal boundary arises from two factors. First, from the molecular architecture, the PBA blocks are anchored on both ends while the PMMA blocks are only anchored at one end. Second, since all the PBA blocks are anchored to a junction point, in our case the MOCs, each PBA block tends to be significantly stretched to relieve the spatial crowding, known as "junction constraint".[68] Thus, the PBA blocks experience more conformational restrictions than the PMMA blocks. This effect is more pronounced when the PBA blocks are short and the number of constrained polymer chains is large. Therefore, the spinodal boundary shifts to lower values at the high f_{PMMA} region (relatively shorter PBA) with increasing arm numbers.

According to this model, the star-shaped polymer architecture can facilitate the self-assembly of the BCPs when (a) the molecular weight of the arm is small, (b) the fraction of the blocks linked to the star core is high, and (c) the number of arms is large. This model qualitatively agrees with our experimental results. For BCPMOCs based on $\mathbf{PMMA_{4k}\text{-}PBA_{19k}}$ and $\mathbf{PMMA_{8k}\text{-}PBA_{48k}}$, which have similar PMMA fractions, the smaller polymer $\mathbf{PMMA_{4k}\text{-}PBA_{19k}}$ BCPMOC showed increased long-range ordering as shown by SAXS, while $\mathbf{PMMA_{8k}\text{-}PBA_{48k}}$ BCPMOC showed no such effect. Because $\mathbf{PMMA_{8k}\text{-}PBA_{27k}}$ has a larger volume fraction of PMMA than $\mathbf{PMMA_{8k}\text{-}PBA_{48k}}$, the BCPMOC based on it also showed enhanced phase separation.

To further expand upon the functionality of BCPMOCs, we investigated the formation of BCPMOC organogels through the use of a selective solvent. Since PMMA has an upper critical

DOI: 10.1021/jacs.6b06712
J. Am. Chem. Soc. 2016, 138, 10708−10715

solution temperature (UCST) in 2-ethyl hexanol solvent,[57] i.e., it dissolves when heated and aggregates when cooled, we envisioned the formation of thermally responsive BCPMOC organogels. We studied the mechanical properties of **$PMMA_{8k}$-PBA_{27k}-L3** derived BCPMOCs in 2-ethyl hexanol as a function of temperature in Figure 6a (purple trace). At low temperatures, G' was greater than G''; the system was a transparent gel. Upon heating, G' significantly decreased and became smaller than G''; the system switched to a viscous solution. Depending on the type of MOC involved, the mechanical properties of the BCPMOC gel varied significantly. When prepared with the same polymer mass fraction, gels with $M_{12}L_{24}$ MOC junctions had a much higher modulus (G' = 6.3 kPa) than ones with M_2L_4 paddlewheel junctions (G' = 0.9 kPa) due to the difference in branch functionality (Figure 6a). These data are consistent with the trend described above for BCPMOCs in the bulk state. The SAXS profile of the gel shows a Bragg peak indicative of the aggregated PMMA domains (d-spacing of 25.4 nm). This peak disappears when the gel is heated; the process is fully reversible (Figure 6b). Pictures of BCPMOCs at 25 and 50 °C are also shown in Figure 6b, inset.

The difference in branch functionalities (24 vs 4) also influenced the spacing between the aggregated PMMA domains in the BCPMOC gels (Figure 6c), which directly affected the UCST. The **L2**-based BCPMOC gels had a d-spacing of 27.3 nm while the **L3**-based BCPMOC gels had a d-spacing of 25.4 nm. Moreover, the sol−gel transition occurred at different temperatures: 27 °C vs 37 °C for the paddlewheel- and sphere-containing BCPMOC gels, respectively.

The stepwise assembly strategy we employ makes it possible to incorporate different MOC junctions into one BCPMOC by simply mixing the preassembled star polymers. Because the type and geometry of the MOC structure dominates the mechanical properties and the UCST, we hypothesized that we could finely tune the materials' properties by adjusting the percentage of different MOC junctions in mixed BCPMOCs. We demonstrate this idea by mixing, at different ratios, star polymers with the spherical MOC junctions and the paddlewheel junctions. As can be seen in Figure 6d (red trace), the stiffness of the mixed BCPMOC gels increased almost linearly as the percentage of spherical MOC core increased. The sol−gel transition temperature also changed with the ratio of different MOC junctions (Figure 6d, blue trace, and Figure S8). To confirm the presence and integrity of the sphere and paddlewheel MOCs in the mixed gels, and to rule out thermally induced exchange of ligands from one MOC type with the other, we carried out a model study with MOCs derived from ligands **L2** and **L3** without BCPs attached. When the materials were mixed at room temperature, ^{1}H NMR showed separate sets of peaks that corresponded to the spherical MOCs and the paddlewheel MOCs (Figure S9). After heating at 50 °C, well above the sol−gel transition temperature, the NMR spectra do not show appreciable changes; heating at 80 °C is required to induce any changes in the MOC structure.

CONCLUSION

Herein, we introduced block co-polyMOCs (BCPMOCs), which are a class of hierarchically structured materials formed via stepwise metallosupramolecular assembly of MOCs followed by BCP microphase separation. We demonstrate that the choice of the MOC, as determined by small differences in the ligand structure, can lead to large differences in the microscopic and mesoscopic structures and mechanical properties of BCPMOCs. Due to the diverse range of MOCs and BCPs that could be employed in the BCPMOC paradigm, we expect that BCPMOCs will offer numerous opportunities for functional materials design.

ASSOCIATED CONTENT

Supporting Information

The Supporting Information is available free of charge on the ACS Publications website at DOI: 10.1021/jacs.6b06712.

Materials, synthetic procedures, characterization methods, and additional notes and figures (PDF)

AUTHOR INFORMATION

Corresponding Author

*jaj2109@mit.edu

Notes

The authors declare no competing financial interest.

ACKNOWLEDGMENTS

We thank the National Science Foundation (CHE-1334703) and Henkel Inc. for support of this work. We are grateful to Prof. N. Holten-Andersen and Mr. Q. Li for helpful discussions. This work made use of the MRSEC Shared Experimental Facilities supported by the National Science Foundation under Award DMR-1419807, as well as the DCIF facility NMR instruments supported by NIH Grant 1S10RR013886-01 and the NSF Grant DBI-9729592.

REFERENCES

(1) Leininger, S.; Olenyuk, B.; Stang, P. J. *Chem. Rev.* **2000**, *100*, 853−908.
(2) Chakrabarty, R.; Mukherjee, P. S.; Stang, P. J. *Chem. Rev.* **2011**, *111*, 6810−6918.
(3) Cook, T. R.; Zheng, Y.-R.; Stang, P. J. *Chem. Rev.* **2013**, *113*, 734−777.
(4) Nitschke, J. R. *Acc. Chem. Res.* **2007**, *40*, 103−112.
(5) Smulders, M. M. J.; Riddell, I. A.; Browne, C.; Nitschke, J. R. *Chem. Soc. Rev.* **2013**, *42*, 1728−1754.
(6) Fujita, M. *Chem. Soc. Rev.* **1998**, *27*, 417−425.
(7) Fujita, M.; Tominaga, M.; Hori, A.; Therrien, B. *Acc. Chem. Res.* **2005**, *38*, 369−378.
(8) Oliveri, C. G.; Ulmann, P. A.; Wiester, M. J.; Mirkin, C. A. *Acc. Chem. Res.* **2008**, *41*, 1618−1629.
(9) Eryazici, I.; Moorefield, C. N.; Newkome, G. R. *Chem. Rev.* **2008**, *108*, 1834−1895.
(10) Stang, P. J.; Olenyuk, B. *Acc. Chem. Res.* **1997**, *30*, 502−518.
(11) Ronson, T. K.; Zarra, S.; Black, S. P.; Nitschke, J. R. *Chem. Commun.* **2013**, *49*, 2476−2490.
(12) Meng, W.; Clegg, J. K.; Thoburn, J. D.; Nitschke, J. R. *J. Am. Chem. Soc.* **2011**, *133*, 13652−13660.
(13) Smulders, M. M. J.; Jiménez, A.; Nitschke, J. R. *Angew. Chem., Int. Ed.* **2012**, *51*, 6681−6685.
(14) Wood, C. S.; Ronson, T. K.; Belenguer, A. M.; Holstein, J. J.; Nitschke, J. R. *Nat. Chem.* **2015**, *7*, 354−358.
(15) McConnell, A. J.; Wood, C. S.; Neelakandan, P. P.; Nitschke, J. R. *Chem. Rev.* **2015**, *115*, 7729−7793.
(16) Fujita, M.; Oguro, D.; Miyazawa, M.; Oka, H.; Yamaguchi, K.; Ogura, K. *Nature* **1995**, *378*, 469−471.
(17) Sun, W.-Y.; Yoshizawa, M.; Kusukawa, T.; Fujita, M. *Curr. Opin. Chem. Biol.* **2002**, *6*, 757−764.
(18) Harris, K.; Fujita, D.; Fujita, M. *Chem. Commun.* **2013**, *49*, 6703−6712.
(19) Lehn, J.-M. *Chem. Soc. Rev.* **2007**, *36*, 151−160.
(20) Chambron, J.-C.; Sauvage, J.-P. *New J. Chem.* **2013**, *37*, 49−57.

DOI: 10.1021/jacs.6b06712
J. Am. Chem. Soc. 2016, 138, 10708−10715

(21) Brown, A. M.; Ovchinnikov, M. V.; Stern, C. L.; Mirkin, C. A. *J. Am. Chem. Soc.* **2004**, *126*, 14316−14317.
(22) Newkome, G. R.; Cho, T. J.; Moorefield, C. N.; Baker, G. R.; Cush, R.; Russo, P. S. *Angew. Chem., Int. Ed.* **1999**, *38*, 3717−3721.
(23) Xie, T.-Z.; Li, J.-Y.; Guo, Z.; Ludlow, J. M.; Lu, X.; Moorefield, C. N.; Wesdemiotis, C.; Newkome, G. R. *Eur. J. Inorg. Chem.* **2016**, *2016*, 1671−1677.
(24) Xie, T.-Z.; Guo, K.; Guo, Z.; Gao, W.-Y.; Wojtas, L.; Ning, G.-H.; Huang, M.; Lu, X.; Li, J.-Y.; Liao, S.-Y.; Chen, Y.-S.; Moorefield, C. N.; Saunders, M. J.; Cheng, S. Z. D.; Wesdemiotis, C.; Newkome, G. R. *Angew. Chem.* **2015**, *127*, 9356−9361.
(25) Xie, T.-Z.; Liao, S.-Y.; Guo, K.; Lu, X.; Dong, X.; Huang, M.; Moorefield, C. N.; Cheng, S. Z. D.; Liu, X.; Wesdemiotis, C.; Newkome, G. R. *J. Am. Chem. Soc.* **2014**, *136*, 8165−8168.
(26) Stadler, A.-M.; Kyritsakas, N.; Graff, R.; Lehn, J.-M. *Chem. - Eur. J.* **2006**, *12*, 4503−4522.
(27) Cook, T. R.; Stang, P. J. *Chem. Rev.* **2015**, *115*, 7001−7045.
(28) Zhou, H.-C.; Long, J. R.; Yaghi, O. M. *Chem. Rev.* **2012**, *112*, 673−674.
(29) Furukawa, H.; Cordova, K. E.; O'Keeffe, M.; Yaghi, O. M. *Science* **2013**, *341*, 1230444.
(30) Furukawa, S.; Reboul, J.; Diring, S.; Sumida, K.; Kitagawa, S. *Chem. Soc. Rev.* **2014**, *43*, 5700−5734.
(31) Stock, N.; Biswas, S. *Chem. Rev.* **2012**, *112*, 933−969.
(32) Cook, T. R.; Vajpayee, V.; Lee, M. H.; Stang, P. J.; Chi, K.-W. *Acc. Chem. Res.* **2013**, *46*, 2464−2474.
(33) Olenyuk, B.; Whiteford, J. A.; Fechtenkotter, A.; Stang, P. J. *Nature* **1999**, *398*, 796−799.
(34) Riddell, I. A.; Smulders, M. M. J.; Clegg, J. K.; Nitschke, J. R. *Chem. Commun.* **2011**, *47*, 457−459.
(35) Sun, Q.-F.; Iwasa, J.; Ogawa, D.; Ishido, Y.; Sato, S.; Ozeki, T.; Sei, Y.; Yamaguchi, K.; Fujita, M. *Science* **2010**, *328*, 1144−1147.
(36) Zhao, C.; Sun, Q.-F.; Hart-Cooper, W. M.; DiPasquale, A. G.; Toste, F. D.; Bergman, R. G.; Raymond, K. N. *J. Am. Chem. Soc.* **2013**, *135*, 18802−18805.
(37) Pluth, M. D.; Bergman, R. G.; Raymond, K. N. *Acc. Chem. Res.* **2009**, *42*, 1650−1659.
(38) Wang, Z. J.; Clary, K. N.; Bergman, R. G.; Raymond, K. N.; Toste, F. D. *Nat. Chem.* **2013**, *5*, 100−103.
(39) Fujita, D.; Ueda, Y.; Sato, S.; Yokoyama, H.; Mizuno, N.; Kumasaka, T.; Fujita, M. *Chem.* **2016**, *1*, 91−101.
(40) Jansze, S. M.; Cecot, G.; Wise, M. D.; Zhurov, K. O.; Ronson, T. K.; Castilla, A. M.; Finelli, A.; Pattison, P.; Solari, E.; Scopelliti, R.; Zelinskii, G. E.; Vologzhanina, A. V.; Voloshin, Y. Z.; Nitschke, J. R.; Severin, K. *J. Am. Chem. Soc.* **2016**, *138*, 2046−2054.
(41) Yan, X.; Li, S.; Pollock, J. B.; Cook, T. R.; Chen, J.; Zhang, Y.; Ji, X.; Yu, Y.; Huang, F.; Stang, P. J. *Proc. Natl. Acad. Sci. U. S. A.* **2013**, *110*, 15585−15590.
(42) Li, Z.-Y.; Zhang, Y.; Zhang, C.-W.; Chen, L.-J.; Wang, C.; Tan, H.; Yu, Y.; Li, X.; Yang, H.-B. *J. Am. Chem. Soc.* **2014**, *136*, 8577−8589.
(43) Hardy, J. G.; Cao, X.-y.; Harrowfield, J.; Lehn, J.-M. *New J. Chem.* **2012**, *36*, 668−673.
(44) Burnworth, M.; Tang, L.; Kumpfer, J. R.; Duncan, A. J.; Beyer, F. L.; Fiore, G. L.; Rowan, S. J.; Weder, C. *Nature* **2011**, *472*, 334−337.
(45) Yan, X.; Cook, T. R.; Pollock, J. B.; Wei, P.; Zhang, Y.; Yu, Y.; Huang, F.; Stang, P. J. *J. Am. Chem. Soc.* **2014**, *136*, 4460−4463.
(46) Yan, X.; Li, S.; Cook, T. R.; Ji, X.; Yao, Y.; Pollock, J. B.; Shi, Y.; Yu, G.; Li, J.; Huang, F.; Stang, P. J. *J. Am. Chem. Soc.* **2013**, *135*, 14036−14039.
(47) Chifotides, H. T.; Dunbar, K. R. *Acc. Chem. Res.* **2013**, *46*, 894−906.
(48) Kawamoto, K.; Grindy, S. C.; Liu, J.; Holten-Andersen, N.; Johnson, J. A. *ACS Macro Lett.* **2015**, *4*, 458−461.
(49) Foster, J. A.; Parker, R. M.; Belenguer, A. M.; Kishi, N.; Sutton, S.; Abell, C.; Nitschke, J. R. *J. Am. Chem. Soc.* **2015**, *137*, 9722−9729.
(50) Zheng, W.; Chen, L.-J.; Yang, G.; Sun, B.; Wang, X.; Jiang, B.; Yin, G.-Q.; Zhang, L.; Li, X.; Liu, M.; Chen, G.; Yang, H.-B. *J. Am. Chem. Soc.* **2016**, *138*, 4927−4937.
(51) Hosono, N.; Gochomori, M.; Matsuda, R.; Sato, H.; Kitagawa, S. *J. Am. Chem. Soc.* **2016**, *138*, 6525−6531.
(52) Zhukhovitskiy, A. V.; Zhong, M.; Keeler, E. G.; Michaelis, V. K.; Sun, J. E. P.; Hore, M. J. A.; Pochan, D. J.; Griffin, R. G.; Willard, A. P.; Johnson, J. A. *Nat. Chem.* **2016**, *8*, 33−41.
(53) BATES, F. S. *Science* **1991**, *251*, 898−905.
(54) Mai, Y.; Eisenberg, A. *Chem. Soc. Rev.* **2012**, *41*, 5969−5985.
(55) Bates, F. S.; Fredrickson, G. H. *Phys. Today* **1999**, *52*, 32−38.
(56) Nese, A.; Mosnáček, J.; Juhari, A.; Yoon, J. A.; Koynov, K.; Kowalewski, T.; Matyjaszewski, K. *Macromolecules* **2010**, *43*, 1227−1235.
(57) Seitz, M. E.; Burghardt, W. R.; Faber, K. T.; Shull, K. R. *Macromolecules* **2007**, *40*, 1218−1226.
(58) Magenau, A. J. D.; Kwak, Y.; Matyjaszewski, K. *Macromolecules* **2010**, *43*, 9682−9689.
(59) Yoneya, M.; Tsuzuki, S.; Yamaguchi, T.; Sato, S.; Fujita, M. *ACS Nano* **2014**, *8*, 1290−1296.
(60) Rubinstein, M.; Colby, R. H. *Polymers Physics*; Oxford University Press, 2003.
(61) Kikuchi, T.; Sato, S.; Fujita, D.; Fujita, M. *Chem. Sci.* **2014**, *5*, 3257−3260.
(62) Pakula, T.; Koynov, K.; Boerner, H.; Huang, J.; Lee, H.-i.; Pietrasik, J.; Sumerlin, B.; Matyjaszewski, K. *Polymer* **2011**, *52*, 2576−2583.
(63) Zhou, H.; Woo, J.; Cok, A. M.; Wang, M.; Olsen, B. D.; Johnson, J. A. *Proc. Natl. Acad. Sci. U. S. A.* **2012**, *109*, 19119−19124.
(64) Sato, S.; Ishido, Y.; Fujita, M. *J. Am. Chem. Soc.* **2009**, *131*, 6064−6065.
(65) Yamazaki, H.; Takeda, M.; Kohno, Y.; Ando, H.; Urayama, K.; Takigawa, T. *Macromolecules* **2011**, *44*, 8829−8834.
(66) Shi, W.; Tateishi, Y.; Li, W.; Hawker, C. J.; Fredrickson, G. H.; Kramer, E. J. *ACS Macro Lett.* **2015**, *4*, 1287−1292.
(67) Delaney, K. T.; Fredrickson, G. H. *Comput. Phys. Commun.* **2013**, *184*, 2102−2110.
(68) Olvera de la Cruz, M.; Sanchez, I. C. *Macromolecules* **1986**, *19*, 2501−2508.

DOI: 10.1021/jacs.6b06712
J. Am. Chem. Soc. 2016, 138, 10708−10715